Characterization and development of an electrical conductivity flow cell for the axial continuous phase fraction profiling of bulk multiphase flow

M R Lepage[1]**, L Vinnett**[1,2]**, C O Gomez**[1]**, O Liboiron-Ladouceur**[3]
and K E Waters[1,4]

[1] Department of Mining and Materials Engineering, McGill University, 3610 University, Montreal, Quebec H3A 0C5, Canada
[2] Departmento de Ingeniería Química y Ambiental, Universidad Técnica Federico Santa María, Valparaíso, Chile
[3] Department of Electrical and Computer Engineering, McGill University, 3480 Rue University, Montreal, Quebec H3A 0E9, Canada

E-mail: kristian.waters@mcgill.ca

Abstract

In this study, the electric field generated by axial ring electrode conductivity cells is investigated. It is shown that the geometric parameters of such cells (mainly electrode separation, diameter and width) have a large effect on the resulting electric field uniformness. To quantify this effect, a parameter termed the effective measurement volume (EMV) is introduced which quantifies the measurement volume within the conductivity cell that contains 90% of the total current, normalized to that of an ideal conductivity cell (which generates a uniform electric field). The effects of a conductivity cells EMV on bulk conductivity measurements are both simulated and experimentally confirmed for emulated annular two-phase flow conditions. The results show that measurements performed with conductivity cells of high EMV tend towards true void fraction values, whereas cells of low EMV tended towards larger measurement error. This is quantified in the sum of squared residuals of the measurement, where a conductivity cell with an EMV of 0.19 has a sum of squared residual that is 638.4 times larger than a cell with an EMV of 1.00. Understanding the limitations of geometric parameters, a new axial conductivity profiling sensor was developed that uses one pair of electric field generating electrodes, and multiple measurement electrodes to create an axial conductivity profile with an axial measurement resolution of 10 mm.

Keywords: conductivity flow cell, axial conductivity profiling, gas concentration measurements

(Some figures may appear in colour only in the online journal)

1. Introduction

Multiphase flows are an essential component of many industrial applications, ranging from mining & mineral processing, to oil & gas, pharmaceuticals and food. The use of conductivity has been widely applied to measure volumetric fractions of different phases in multiphase flow. Conductivity measurements have been applied to oil–water [1], solid-water flows [2], foams for food research [3], froth flotation machines [4], and thickeners [5], among others. Mineral processing is the concentration of valuable minerals found in an ore, to a concentration that is practical for metal production through smelting or

hydrometallurgical routes (there are instances when the concentrated mineral is the final product, for example industrial minerals such as talc), with the main separation method in use being 'flotation'. In flotation, the main recovery mechanism of valuable mineral comes from the attachment of minerals to rising air bubbles, thus the concentration of air in a flotation machine is of importance [6] (for more information on mineral processing and flotation, readers are suggested to consult Wills and Finch [7]). Maxwell's model [8] has been successfully applied to mineral flotation to measure the concentration of gas (dispersed phase), often termed the gas holdup. The design of a conductivity cell to measure flotation gas concentration began with Uribe-Salas *et al* [9] who applied a pair of grid electrodes, perpendicular to the axial axis of a flotation column to measure the solid and gas concentration in water–solid and water–air systems, respectively. Banisi *et al* [10] extended the use of axial grid electrodes and showed that the gas concentration could be accurately measured in three-phase systems by considering the solid and water phases as a single continuous phase. To measure the gas concentration in industrial flotation machines, Miranda [11] introduced the use of ring electrodes, flush to the wall of a cylindrical polyvinyl chloride (PVC) pipe. To limit the loss of current to grounded sources within the flotation machine (such as the metal walls of the machine), the exciting electrode was surrounded by two grounded rings [11]. Cortes-Lopez [12] developed a s*yphon cell*, which measured just the continuous phase. This allowed both the bulk and continuous conductivities to be measured simultaneously, thus giving the gas concentration whilst requiring no assumptions to be made regarding the operating conditions—this was achieved in-situ in a flotation machine. The use of this sensor has been used extensively in industrial flotation diagnostics [4].

In the flotation froth zone, the concentration of gas is much larger, typically in the range of 70%–90% gas [13]. Marchese *et al* [14] showed that Maxwell's model deviates at a gas concentration larger than 50%. Feitosa *et al* [15] revisited the relationship of relative conductivity to gas concentration and proposed an empirical model that covers the full range of void concentrations for two phase (water–air) dispersions. Of particular interest in the application to froth flotation, is the change in gas concentration in the axial-dimension for flotation froths. As the height of the froth increases, water begins to drain from the froth, which has implications on the overall performance of flotation [16]. Achieving a reasonable axial measurement resolution requires closely spaced conductivity electrodes which brings into question how the measurement of bulk conductivity is affected by electrode geometry. The basis of all models relating dispersion conductivity to the phase concentrations is an accurate bulk conductivity measurement of the dispersion. The accuracy of bulk conductivity measurements must consider the uniformity of the electric field generated by the geometry of the electrodes, which will be discussed in this study. As explored in this work, if the electrodes are spaced very close together, the current is concentrated very close to the outer edge of the conductivity cell and a poor bulk conductivity measurement is achieved. Knowing exactly at what electrode diameter to separation length is required to achieve

a good bulk conductivity measurement allows the design of good axial conductivity measurement. This study explores two subjects, the effects of the cell geometry and the resulting electric field on the bulk conductivity measurement and applying this knowledge to develop a new axial conductivity sensor with an axial measurement resolution of 10 mm.

2. Theoretical considerations

2.1. Conductivity measurements and the electric field

The current density, $\vec{j}$ (A · mm^{-2}) inside a conductivity cell is related to the conductivity of the solution, κ (mS · mm^{-1}), and the electric field, $\vec{E}$ (A · mm^{-1}), by Ohm's law in equation (1). The analysis is performed assuming a static magnetic field, and motional electromotive forces are assumed negligible.

$$\vec{j} = -\kappa \, \vec{E} \tag{1}$$

where the electric field is defined by the electric potential gradient produced by the geometry of the electrodes defined in cylindrical coordinates in equation (2):

$$\vec{E} = -\nabla \varphi = -\frac{\partial \varphi}{\partial r}\hat{r} + \frac{1}{r}\frac{\partial \varphi}{\partial \phi}\hat{\phi} + \frac{\partial \varphi}{\partial z}\hat{z} \tag{2}$$

where φ (V) is the electric potential, and $\hat{r}$, $\hat{\phi}$ and $\hat{z}$ are unit vectors.

In the derivation of fundamental models of conductivity theory, the electric field is assumed to be uniform, which is generated under three ideal cell configurations [9]:

1. Two infinite parallel plate electrodes
2. Two infinite concentric cylindrical electrodes
3. Two concentric spherical electrodes

Under these conditions, the contribution to the measurement of any point within the conductivity cell is equal, thus considered ideal for bulk conductivity measurements. These cell configurations are, however, impractical—especially when measuring the axial change in a flowing solution without interrupting the flow. Deviations from these cell configurations produce a non-uniform electric field. This creates areas of higher and lower current density between the electrodes, resulting in areas that contribute more to the measurement than others. From this, the non-uniformity of the electric field generated by a given electrode configuration must be considered when assessing the accuracy of the bulk measurement. In literature, investigations into electric field uniformity stem primarily from the measurement of three phase oil-water–gas systems in oil wells. Andreussi *et al* [17] investigated different spacing between ring electrodes under dispersed bubble flow conditions (similar to conditions experienced in a flotation machine) and determined that Maxwell's model only applied when the electrodes were spaced far apart. They remarked (qualitatively) that the bubbles were mainly located close to the axis of the ring electrodes, thus alluding to an issue with the electric field generated when the rings were spaced close together. Devia and Fossa [18] solved the Laplace equation to simulate different spacing between ring electrodes,
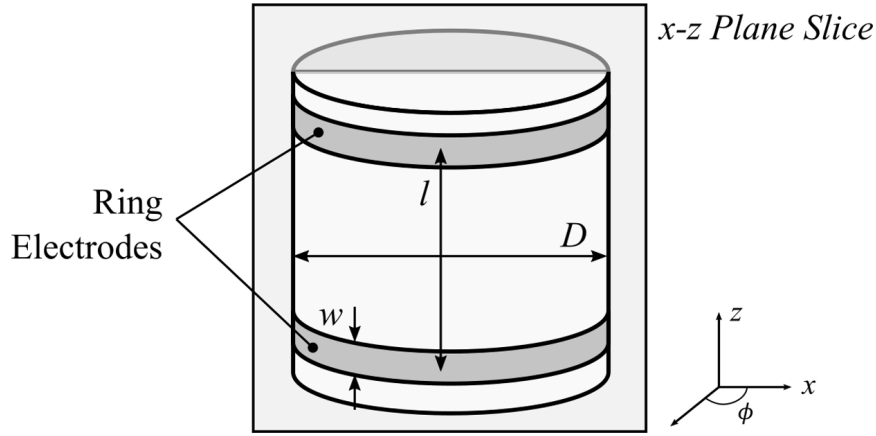
x-z Plane Slice

Figure 1. Geometry of the ring electrode conductivity cell. The following analysis has the cell geometry: $D = 100\,mm$, $l = 30\,mm$, $w = 10\,mm$.

and determined that by increasing the electrode distance, the response approached that predicted by the Bruggeman curve [19] under dispersed bubbly flow. This, therefore, indicated a good bulk dispersion measurement. To explain this phenomenon, Jin *et al* [20] investigated the electric field and defined quantitative parameters to measure the electric field uniformness. The field uniformness parameter was split into axial and radial uniformness. Using this criterion, the effect of electrode height and separation were investigated. It was determined that as the electrode height increased, the radial field uniformity decreased, while the axial uniformity remained unchanged. The electrode separation was shown to enhance the uniformity of the electric field. This study investigates and extends the idea of quantifying the electric field uniformness parameter by introducing a single normalized value, termed the effective measurement volume (EMV) for a ring electrode conductivity sensor. The effects of electrode separation, width and diameter on the electric field uniformness were simulated using finite element analysis. The effect of the EMV on the accuracy of bulk heterogeneous conductivity measurements are simulated and experimentally shown.

3. Methodology

3.1. Simulating the electric field

The focus of this study is on ring electrode conductivity cells, which can be easily applied to cylindrical pipes and are non-intrusive and thus, do not disrupt the dispersion flow being measured. To measure conductivity, an electric field is generated between two electrodes, where one electrode is the current injecting electrode and the other is grounded. For visualization purposes, a conductivity cell consisting of two $100\,mm$ diameter (D) ring electrodes, with a width (w) of $10\,mm$, spaced (l) $30\,mm$ apart (midpoint to midpoint) is investigated in the following simulation (figure 1):

The electric field is simulated using the finite element analysis in MATLAB's Partial Derivative Equation Toolbox version 3.2 [21]. Assuming a homogenous conductivity, and that the only current generation is at the current injection

electrode, equation (4) can be reduced to a general form of the Laplace equation that describes the resulting potential field, φ (V), generated between the electrodes (equation (3)):

$$\nabla^2 \varphi = 0. \tag{3}$$

Equation (8) can be solved by setting the boundary conditions of the system. The rings are set flush to the walls of an electrically insulating PVC pipe, where the Neumann boundary condition is described by equation (4):

$$\overrightarrow{n} \cdot (\kappa \nabla \varphi) = 0 \tag{4}$$

where $\overrightarrow{n}$ is the normal unit vector directed towards the PVC pipe. Due to cylindrical symmetry, the solution of equation (3) can be reduced to a plane slice, which is shown in figure 2:

The current density streamlines shown in figure 2 are described by equation (5):

$$\overrightarrow{j} = -\kappa \left(\frac{\partial \varphi}{\partial x} \hat{i} + \frac{\partial \varphi}{\partial z} \hat{k} \right) \tag{5}$$

where $\hat{i}$ and $\hat{k}$ are unit vectors.

The distribution of the current density is of particular interest as it shows where the current is the strongest. To generalize the solution, the magnitude of the current density is normalized to the maximum magnitude current density in the region of interest by equation (6) and shown in figure 3:

$$\left\| \overrightarrow{j_n} \right\|_{x,z} = \frac{\left\| \overrightarrow{j} \right\|_{x,z}}{\left\| \overrightarrow{j} \right\|_{max}} \tag{6}$$

where $\left\| \overrightarrow{j_n} \right\|_{x,z}$ is the normalized current density magnitude at a point, $\left\| \overrightarrow{j} \right\|_{x,z}$ is the current density magnitude at a point, and $\left\| \overrightarrow{j} \right\|_{max}$ is the maximum current density magnitude in the domain.

The magnitude of the current density is shown to vary radially, with large spikes at the edge of the electrode surfaces. The information about conductivity gathered from the solution
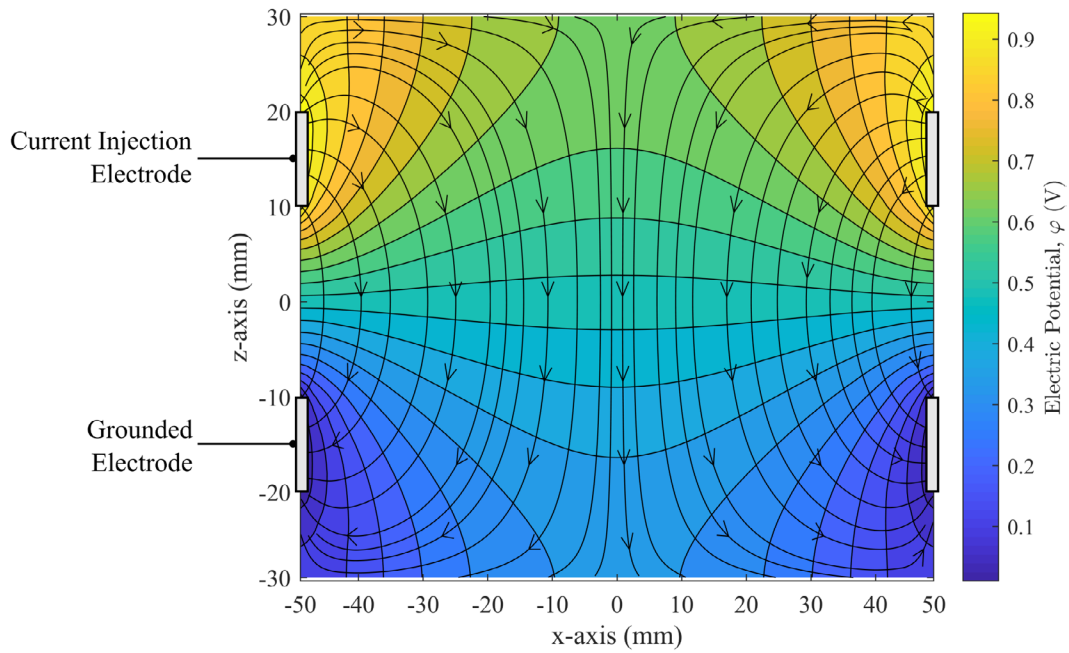
Figure 2. Electric potential field generated by the ring electrode conductivity cell. $D = 100\,\text{mm}$, $l = 30\,\text{mm}$, $w = 10\,\text{mm}$. Current density streamlines are included (lines with arrows) to show the path of current. The two conductivity electrodes are overlaid as shown.
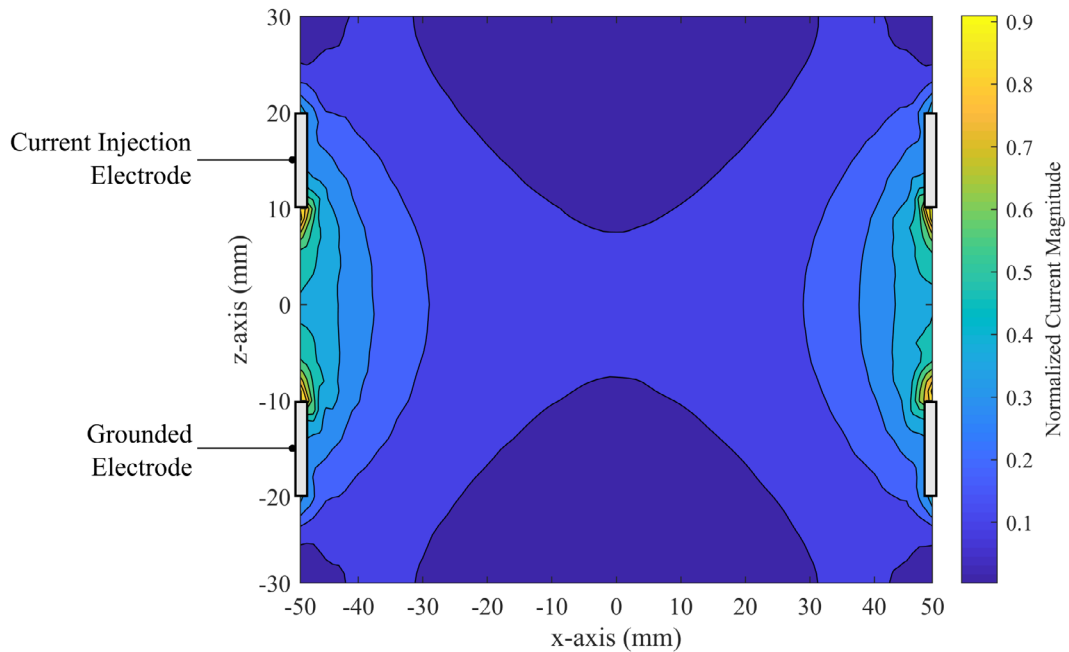

Figure 3. Relative current magnitude generated by the ring electrodes of the conductivity cell. $D = 100\,\text{mm}$, $l = 30\,\text{mm}$, $w = 10\,\text{mm}$. Conductivity electrodes are shown at $x = \pm D/2$, $z = \pm l/2$.

is directly related to the magnitude of the current flow. More information is gathered in areas of high current flow [20]. From this, it is shown that the conductivity information is concentrated near the walls of the cell. This is not an issue when measuring a homogenous solution, where the conductivity does not change in the spatial domain. In the measurement of multiphase flow, certain phases with different conductivities can concentrate in local areas, and thus it is important to get a localized bulk conductivity measurement of the dispersion when inferring relative phase concentrations. The next section will discuss

a quantitative method for describing the variance in current within a ring electrode conductivity flow cell.

3.2. Concept of EMV

The EMV quantifies the variation in current density produced by the geometry of the electrodes in a conductivity flow cell. The EMV is defined as being the sensor volume by which 90% (arbitrarily chosen to contain a substantial amount of current) of the total current is contained, when compared to
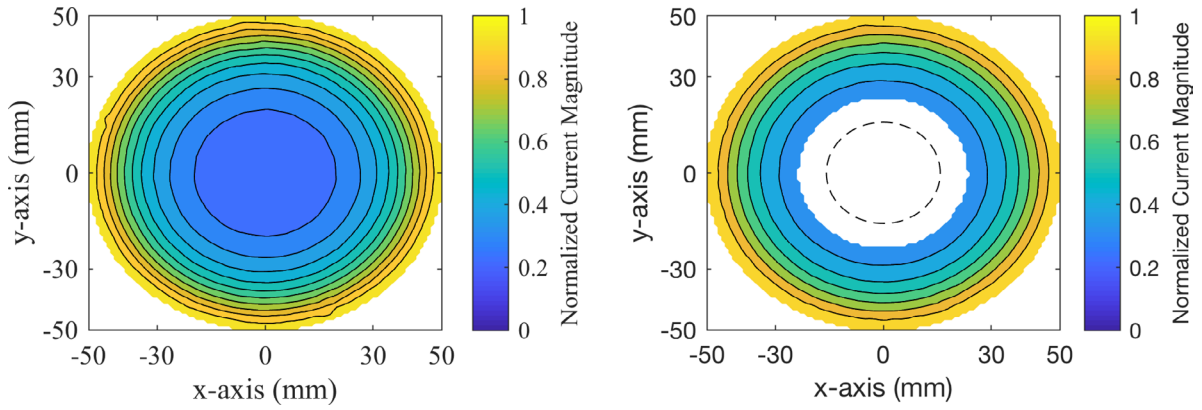
Figure 4. (a) Cross-section at $z = 0$ mm of the relative current density produced by the cell in figure 3. (b) Cross section at $z = 0$ mm of the relative current density after removing the lowest 10% of the total current flowing in the z direction (white area). Dotted line shows thresholding of a uniform field for reference.

that of a uniform electric field. In a uniform electric field, the current is equally distributed and thus is the reference to an ideal bulk measurement. For instance, a sensor that has a poor current distribution will concentrate 90% of the current in a volume smaller than 90% of the total volume. The purpose of this metric is to get an idea of the volume of the sensor that contains meaningful current that contributes significant information about the conductivity. An example of EMV is derived using the electrode geometry from figure 2. First, a *z*-slice is taken at the axial midpoint between the two ring electrodes ($z = 0$ mm from figure 2). The axial midpoint between the electrodes is chosen to minimize the discontinuity effects of the electrodes on the analysis. As the net migration of current density occurs only in the *z*-direction, the total current passing through the *x*–*y* plane at $z = 0$ mm, $I_{z=0}$, is generalized by equation (7):

$$I_{z=0} = \oint \vec{n} \cdot (\kappa \nabla \varphi) \, d\vec{S} \quad [\text{Ampere}]. \quad (7)$$

Knowing the total current passing through the *z*-slice surface, the threshold of 90% is applied which essentially removes 10% of the total current, removing the areas with the lowest current density. The *z*-slice and post threshold *z*-slice are shown in figures 4(a) and (b).

For this analysis (and all conductivity cells containing axial ring electrodes), the lowest current density exists at the center of the sensor, and thus is removed. The area is then compared to that of an ideal cell where the field is uniform. Under a uniform field, the current density has no variance, and thus the 90% threshold removes 10% of the total sensor volume, shown by the dotted line in figure 4(b). The effect is essentially a normalization that produces an EMV value between 1 and 0. As the EMV approaches a value of 1, the electric field generated by the geometry of the electrodes approaches uniformity and thus provides ideal conditions to perform bulk measurements. An EMV that approaches a value of 0 indicates that most of the current is contained near the outer radius of the sensor and thus does not provide the environment for accurate bulk measurement. To summarize, the procedure to calculate the EMV is as follows:
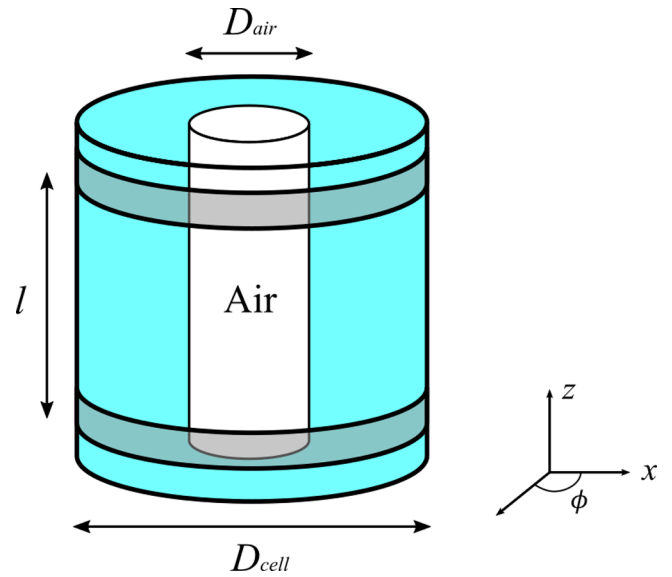

Figure 5. Visualization of simulated air column in water, used to investigate the effects of EMV on resulting bulk conductivity measurement.
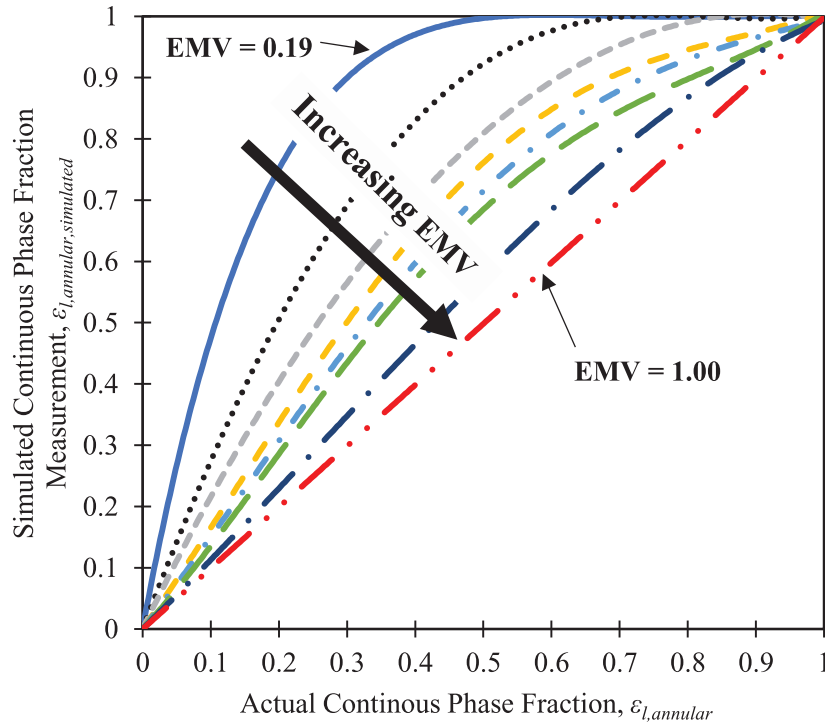
1. Select the *z*-dimension midpoint ($z = 0$ mm) between the current injection and ground electrode.
2. Calculate the total *z*-dimension current flowing through the slice using equation (7).
3. Apply a threshold (90% in this case) to the *z*-dimension current that removes the sensor area with a current density below the threshold.
4. Normalize the resulting area to that of a uniform field, producing an EMV between 1 and 0, where 1 represents a uniform field.

3.3. Effect of EMV on bulk dispersion phase concentration measurements

To show the effects the EMV has on resulting bulk void fraction measurements, an annular flow system is emulated by placing a cylinder of air in water on the center axis of the conductivity sensor (figure 5). Annular flow conditions create
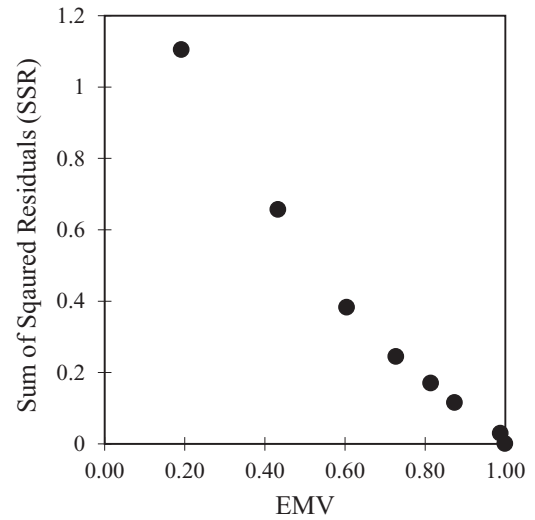
Table 1. Summary of electrode separations and resulting EMV values.

Electrode separation (l) (mm)	10	20	30	40	50	60	120	300
EMV	0.19	0.43	0.60	0.73	0.81	0.87	0.99	1.00

Figure 6. Effect of EMV on simulated continuous phase fraction measurements using air cylinders of varying diameter placed in the center of the sensor.

large radial changes in conductivity, in this case with water (significant conductivity) on the outer edges, with air (effectively nonconductive) at the center axis of the sensor. As shown in section 3.2, the flow of current tends to the outer edges of the conductivity cell and thus a poorly designed conductivity cell (with a low EMV) should show a measurement bias towards the water along the outer edge. This will result in a measurement that over predicts the continuous phase fraction. A well-designed conductivity cell (with an EMV approaching 1) should produce a measurement that tends towards the true void fraction. To test this, the annular flow system is simulated. The conductivity of air, κ_{air}, is assumed to be 0.0 mS cm^{-1}, while the conductivity of the water, κ_{water}, is set to 0.330 mS cm^{-1} (Montréal city water measured by a CDM210 Meter Lab laboratory conductivity meter). The conductivity sensor simulated consists of two 100 mm diameter (D_{cell}) ring electrodes, 5 mm wide (w). To create different EMV values, the spacing (l) of the electrodes varied from 10 to 300 mm, with the resulting EMV values summarized in table 1. To create a wide range of void fractions, the diameter of the air column (D_{air}) varies from 5 mm to 95 mm, creating a range of void fractions of 0.10–0.99, visualized in figure 5.

To simulate the resulting void fraction measurement, the electrodes were set at a voltage of 1 V and 0 V (ground), and the current, I (A), is determined by summing the total current density at the surface of the grounded electrode generalized by equation (8):

Figure 7. The sum of squared residuals for the simulated measurements for the EMV values simulated in figure 6.

$$I = \iint_S \overrightarrow{\boldsymbol{n}} \cdot (\kappa \nabla \varphi)\, \mathrm{d}\, \overrightarrow{\boldsymbol{S}} \qquad (8)$$

where S is the surface of the grounded electrode. The simulated resistivity measurement, G (mS), is then calculated by Ohm's law by equation (9):
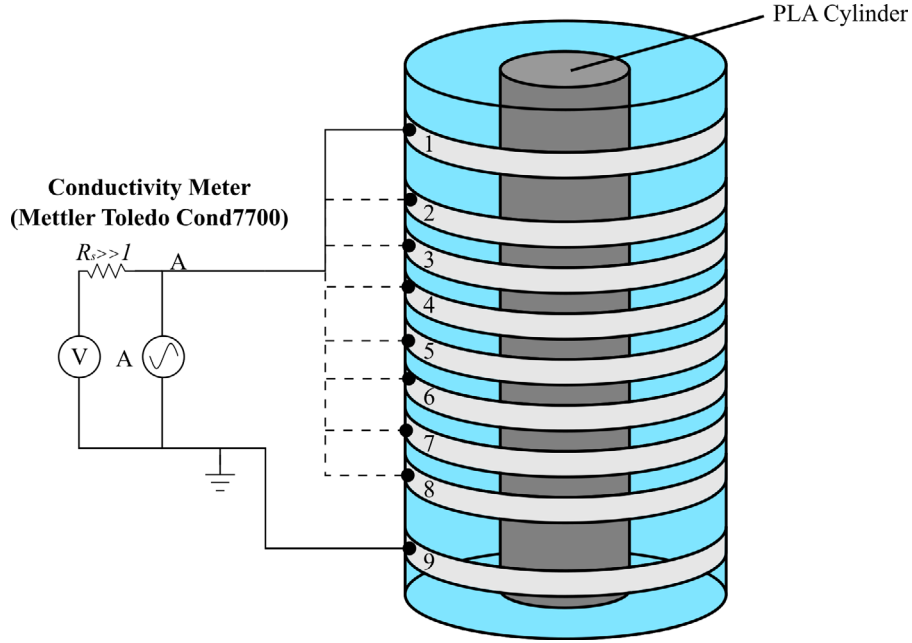
Figure 8. Experimental setup to validate the simulation results from figure 6. The solid line shows the active connection. The dashed line shows the available connections.

Table 2. Summary of electrode separations and resulting EMV values.

Active electrodes (from figure 8)	2,3	2,4	2,5	2,6	2,7	2,8	1,9
Electrode separation (l) (mm)	10	20	30	40	50	60	120
EMV	0.19	0.43	0.60	0.73	0.81	0.87	0.99

$$G = \frac{I}{V}. \tag{9}$$

Where V is the voltage drop across the electrodes. The relative conductivity, K, can then be expressed by equation (10) using the simulated annular phase resistivity, G_{bulk} and continuous phase resistivity, $G_{continuous}$.

$$K = \frac{G_{bulk}}{G_{continuous}}. \tag{10}$$

For annular phase distribution, the continuous phase concentration, $\varepsilon_{l,annular}$, is given by equation (11) [17]:

$$\varepsilon_{l,annular} = K. \tag{11}$$

The effect of the EMV on the resulting simulated continuous phase fraction measurement is shown in figure 6, where the actual continuous phase fraction is calculated by the diameters of the air cylinder (D_{air}) and conductivity cell (D_{cell}) (equation (12)).

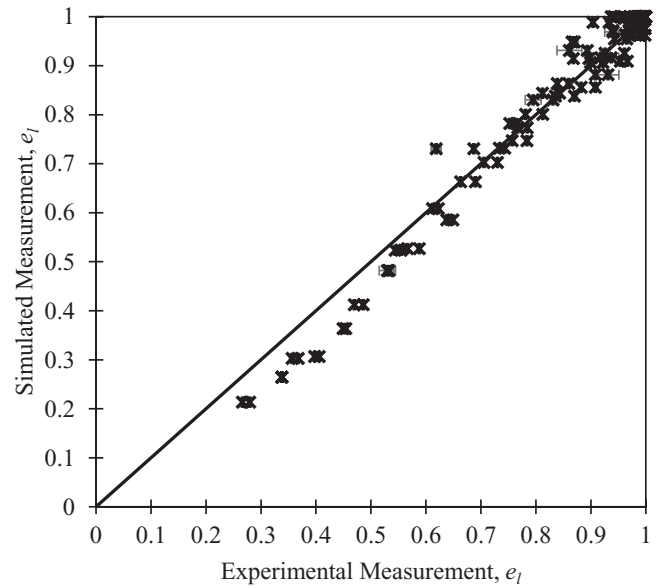$$\varepsilon_{l,actual} = \frac{D_{air}^2}{D_{cell}^2}. \tag{12}$$

Figure 9. Validation of simulation results from figure 6 using experimental data. Error bars are 95% confidence intervals on the experimental measurements.

Table 3. Range of geometric parameters investigated for a ring electrode flow cell.

Geometry parameter	Range
Ring diameter, D	10–500 mm
Ring width, w	1–45 mm
Ring separation, l	5–50 mm

The sum of squared residuals, calculated by equation (13), for the measurements at each calculated EMV are shown in figure 7.
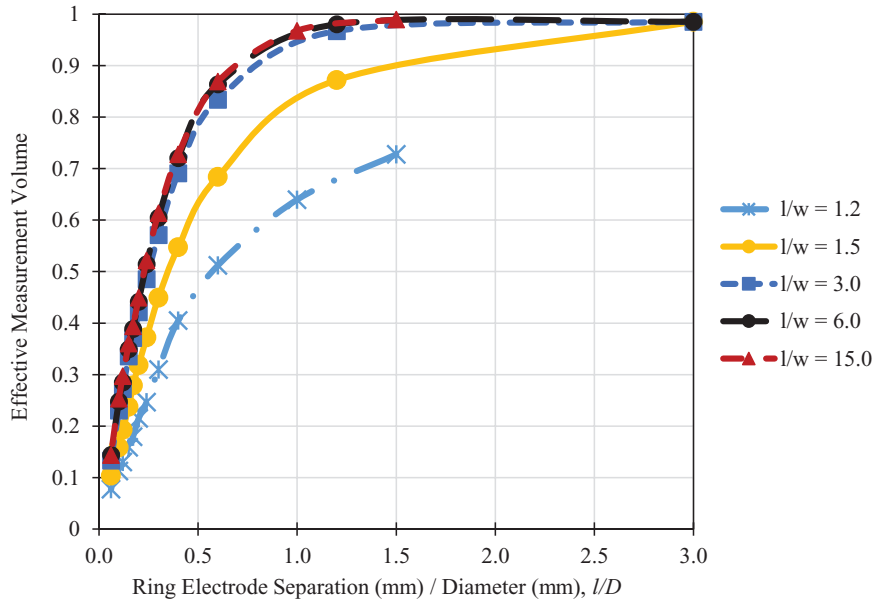
Figure 10. The effect of electrode separation-to-diameter ratio (*l/D*) and length-to-width ratio (*l/w*) on the EMV. Electrode separation (*l*) is fixed at 30 mm.

$$\text{SSR} = \sum_{i=1}^{n} \left(\varepsilon_{\text{l,annular,simulated,i}} - \varepsilon_{\text{l,actual,i}} \right)^2. \quad (13)$$

As the EMV approaches 1, the simulated continuous fraction measurement approaches unity with the actual value. As the electrode separation decreases, the flow of current is more concentrated near the outer edge of the sensor volume, resulting in a decreasing EMV value. Due to the high concentration of current near the outer edge of the conductivity cell, the resulting bulk measurement produces a larger continuous phase fraction than what is actual, as shown in figure 6. While this analysis was performed with an air cylinder, the results can be applied to any radial variance in conductivity, the conclusions being that the EMV should be maximized to provide an effective bulk measurement of continuous or void fractions.

3.4. Validation of the effect of EMV on the measurement of two-phase water content

To validate the effect of the EMV on the measurement of water content, cylinders of varying diameter (20–80 mm, in 10 mm increments) were constructed from polylactic acid (PLA) to emulate the air cylinders investigated in section 3.3. The reported conductivity of PLA is in the range of 10^{-13}–10^{-10} S cm^{-1} [22], a similar order of magnitude to that of air, reported in the range of 10^{-11}–10^{-17} S cm^{-1} [23]. A ring electrode conductivity cell ($D = 100$ mm, $w = 5$ mm) is developed (figure 8), which allows for different spacing of electrodes, producing the different electrode spacing and EMV values matching those simulated in table 1. The different spacing of electrodes is achieved by manually changing which electrodes are connected to the conductivity meter. A summary of the active electrodes and corresponding electrode spacing and EMV values are summarized in table 2.

The conductivity cell is connected to a modular transmitter (M 700, manufactured by Mettler Toledo) with a conductivity module (Cond7700) with a resistivity range from 0.00 kΩ cm–999 MΩ cm and equipped with dynamic electrode polarization prevention. The PLA cylinders are placed on the center axis of the conductivity sensor, with the full experimental setup shown in figure 8.

The experimental measurements were compared to simulation results, shown in figure 9.

The experimentally measured water content readings matched the measurement bias seen from the simulations presented in figure 6, thus indicating that the EMV can be used to quantify a conductivity cells ability for bulk conductivity measurement and, in turn, relative phase concentration measurements.

4. Results and discussion

4.1. Effect of electrode geometry on EMV

For a ring electrode geometry, three parameters were investigated: the electrode ring diameter, D (mm), ring width, w (mm), and ring midpoint separation, l (mm) as illustrated in figure 1. These geometric parameters are varied in the ranges indicated in table 3. For all simulations, the ring electrodes were set to a potential of 1 V, with the other grounded. The outer walls of the conductivity cell are assumed to be electrically insulated.

The effect of changing the electrode ring diameter on the EMV for different electrode widths is shown in figure 10. The ring separation is fixed at 30 mm, producing different electrode separation-to-diameter (*l/D*) and separation-to-width (*l/w*) ratios.

Increasing the electrode diameter, while keeping the separation constant produces a decreasing separation-to-diameter
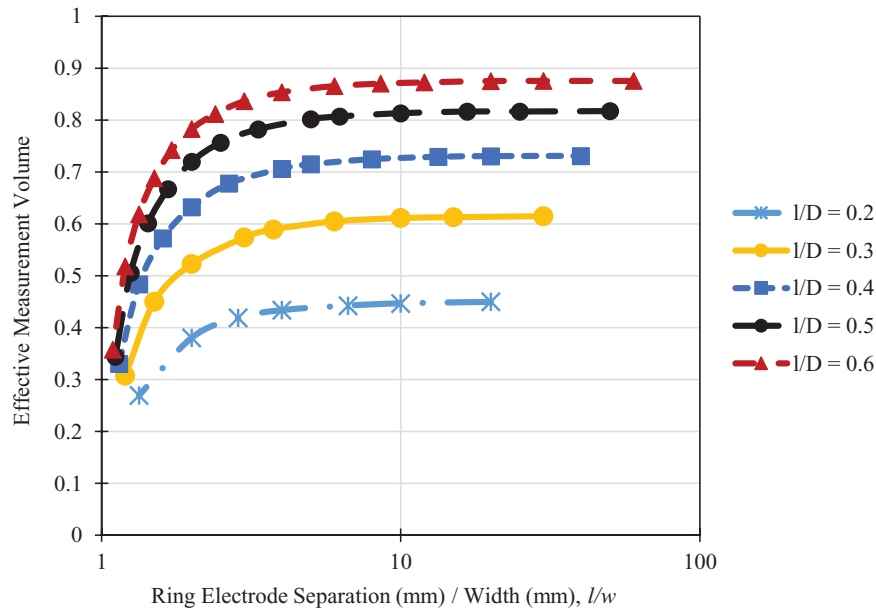
Figure 11. Effect of electrode separation-to-width (l/w) and separation-to-diameter (l/D) ratios on the EMV. The electrode diameter (D) is fixed at 100 mm.
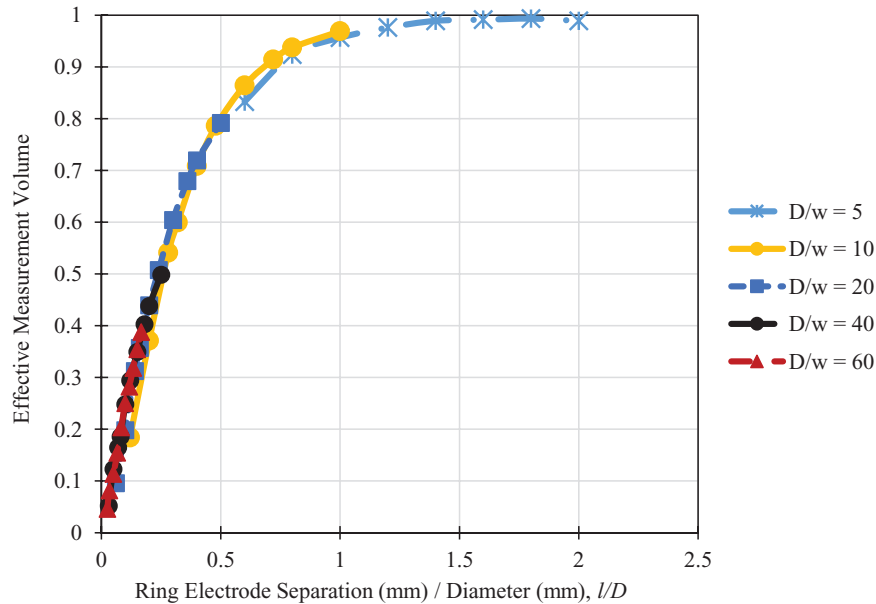

Figure 12. Effect of electrode separation-to-diameter (l/D) and diameter-width (D/w) ratios on the EMV for different electrode diameters. The electrode width is fixed at 5 mm.

ratio, which is shown in figure 10 to have a large effect on the EMV. As the ring diameter decreases, the EMV approaches 1. The effect of electrode width is shown to be negligible at larger separation-to-width ratios ($l/w > 3.0$) and decreases significantly the EMV at smaller ratios ($l/w < 3.0$). Larger electrode diameters produce lower EMV value, indicating a concentration of current along the sensor walls. From these results, the electrode separation-to-diameter ratio should be maximized, taking into consideration the diameter of the pipe or column required for the flow being measured. The diameter of the electrodes should be sufficiently large to measure a true bulk conductivity, avoiding the influence of local variations (e.g. be sufficiently large to avoid the influence of large air

bubbles moving through the sensor). For a sufficiently large separation-to-width ratio ($l/w > 3.0$), a separation-to-diameter ratio is recommended to be no less than 1.0, which would produce an EMV value of ~0.97.

The effect of changing the electrode ring width on the EMV is further investigated at different ring separations and a constant diameter of 100 mm, producing different electrode separation-to-width (l/w) and separation-to-diameter (l/D) ratios, shown in figure 11.

An increasing electrode ring separation-to-width ratio is shown to increase the EMV. It is also shown that as the electrode separation-to-diameter ratio decreases, the resulting EMV decreases as well, as predicted in figure 10. The effect
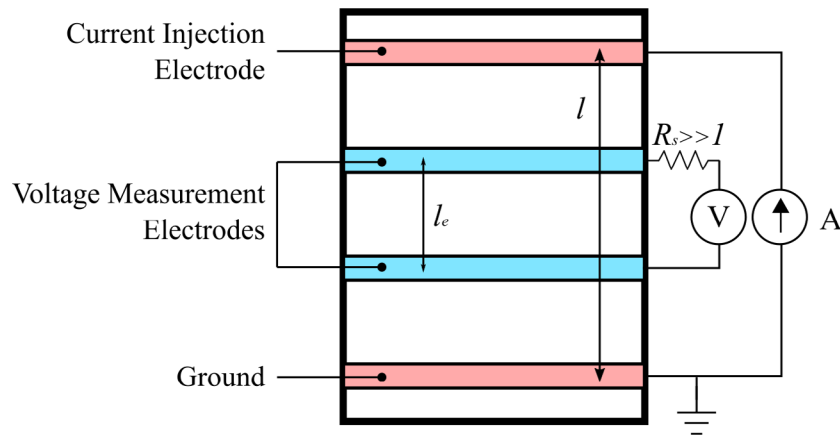
Figure 13. Simplified schematic of a four-electrode conductivity cell. The outer electrodes are the current injection pair, while the inner electrodes are the voltage measurement electrode pair.

of the electrode width is explained by the apparent decrease in separation between the edge of the electrodes. Consider the case of an electrode pair with a midpoint spacing of 60 mm, when the width of the electrode is 10 mm, the separation from the edge of each electrode is 50 mm. However, when the width of the electrode is increased to 50 mm, the edge to edge separation of the electrodes has been reduced to just 10 mm. This apparent decrease in electrode separation effectively reduces the separation between the electrodes, which decreases the resulting EMV. From this, the smallest practical electrode width should be used to maximize the EMV for any given electrode geometry (ignoring other practical implications). This effect is further investigated in figure 12, where the electrode width is fixed at 5 mm, and the electrode separation and diameters are changed to produce different electrode diameter-to-width (D/w) and separation-to-diameter (l/D) ratios.

A similar trend is seen as in figure 10, that as the electrode separation-to-diameter ratio increases, the resulting EMV increases. The effect of D/w is shown to have no effect on the general l/D trend as seen in figure 10. Noting that as the electrode width is fixed at 5 mm and the electrode separation was changed, different l/w ratios were produced. It is shown in figure 12 that this l/w has no effect on the general trend. This further confirms that the electrode width only decreases the apparent electrode separation, and thus electrode width should be minimized to practical limitations.

4.2. Development of a conductivity sensor to obtain an axial water content profile

To obtain a vertical profile of the froth zone water content, the profile resolution is limited to how close the electrodes are separated. For example, to obtain a profile with 10 mm axial-dimension resolution, the rings must have a 10 mm separation. To obtain a reasonable EMV value, the ring diameter would need to be less than 10 mm (a l/D ratio of 1.0 producing an EMV of ~0.97 from figure 10) and thus shows a fundamental limitation to the resolution of this measurement. To obtain a large EMV, and thus an accurate bulk measurement, the electrodes must have a sufficiently large separation-to-diameter ratio. A solution to this is to use separate electrode pairs: one
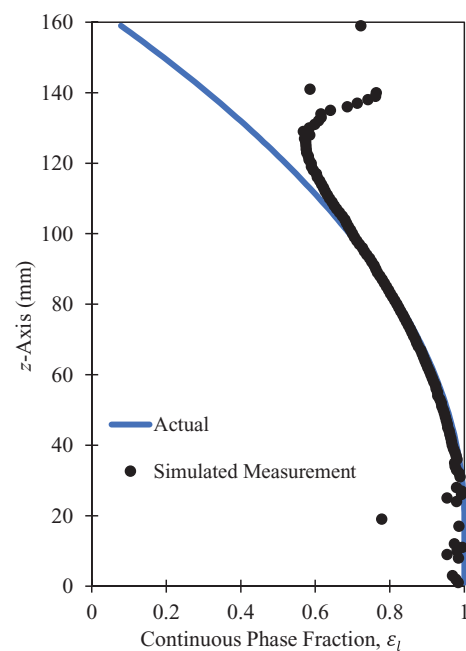

Figure 14. Simulated continuous phase fraction readings based on the voltage drop measured on the outer edge of the conductivity sensor.

pair to inject the current and create the electric field, which can be spaced far apart (l), and the other pair spaced closely together (l_e) to measure the voltage drop across the field to do the conductivity measurement, a schematic of which is shown in figure 13:

A voltage drop is measured across the measurement electrodes, which (ideally) draw no current and thus have little to no effect on the electric field [24]. This allows the measurement electrodes to be placed as close together as required and allows the current injecting electrodes to be spaced with a large separation, generating a high EMV. A four-electrode conductivity cell geometry was simulated, with the current injecting ring electrodes spaced 120 mm (l), 100 mm diameter (D) and 5 mm width (w), with an l/D ratio of 1.2, generating an EMV of 0.99. The greater separation of the current injecting electrodes creates a near uniform electric field between the current injecting electrodes. Measurement electrodes can be
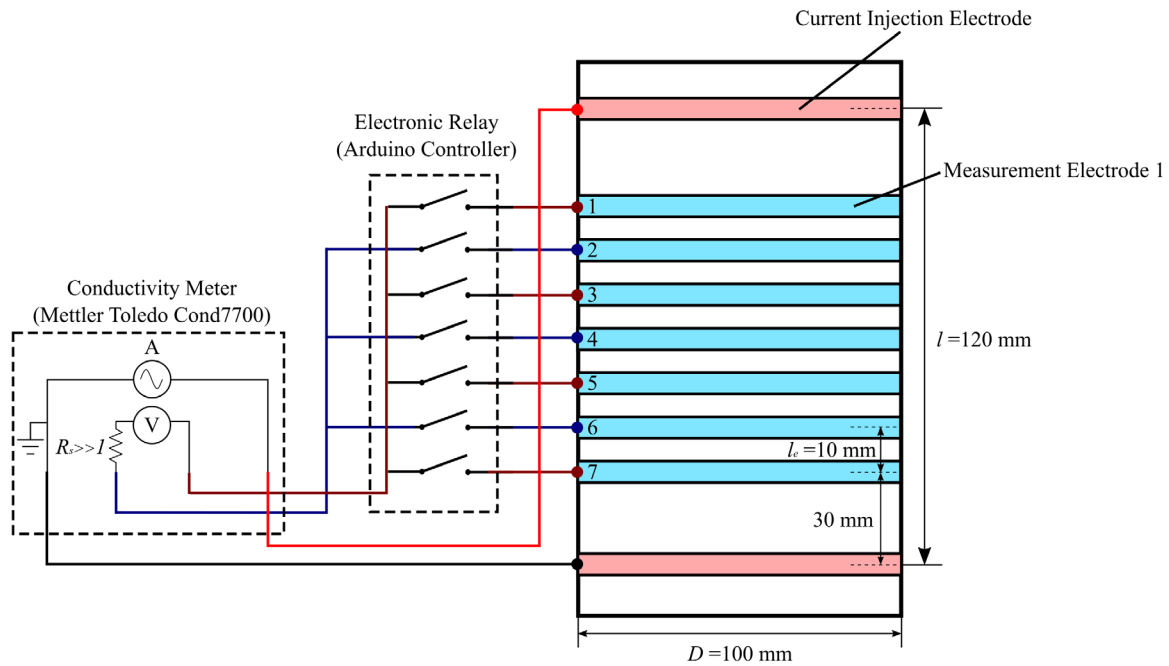
Figure 15. Simplified schematic of the axial profiling conductivity sensor. Red electrodes are current injection, blue electrodes are voltage measurement.

placed anywhere within the field and are only required to measure the voltage drop across the electrode pair. The relative conductivity measurement is reduced down to simply the ratio of voltage drops of the continuous phase and dispersion measurements, shown in equation (14).

$$K = \frac{V_{\text{cont}}}{V_{\text{bulk}}} \qquad (14)$$

where V_{cont} is the voltage drop measured of the continuous phase, and V_{bulk} is the voltage drop measured of the dispersion, across a pair of measurement electrodes. The relative conductivity can then be used to determine the continuous phase fraction by equation (11). A full derivation can be found in appendix.

To generate a conductivity profile in the axial-dimension, multiple pairs of measurement electrodes can be used. For example, to generate a measurement profile with 10 mm resolution, multiple 5 mm width measurement electrodes can be spaced 10 mm apart. To investigate this, a cone of air of known dimensions is placed on the center axis of the conductivity cell and the resulting potential field is simulated by the methodology outlined in section 3.1. A cone was used to generate a continuous phase fraction (and thus effective conductivity) profile that varies in the z-dimension. Figure 14 shows the simulated continuous phase fraction reading, based on the potential drop along the inside of the outer diameter of the sensor (where the measurement electrodes are placed) and equation (14). The simulation was interpolated to a bin size of 1 mm, allowing the voltage drop, and thus continuous phase fraction to be calculated every 1 mm. The midpoints of the current injection pair electrodes are located at $z = 20$ and $z = 140$.

The effect of the current injection electrodes is seen as large deviations from the actual continuous phase fraction and thus

Table 4. Summary of electrode pairs for experimental measurements in figure 16.

Measurement #	Active electrodes (from figure 15)	Measurement midpoint, z (mm) (in figure 16)
1	1,2	105
2	2,3	95
3	3,4	85
4	4,5	75
5	5,6	65
6	6,7	55

limits how close the measurement electrodes can be placed to the current injecting electrodes for accurate measurement.

A conductivity cell is then constructed using nine 5 mm width, 100 mm diameter electrodes. The two current injecting electrodes are spaced 120 mm apart (l), with the seven measurement electrodes spaced 10 mm apart (l_e). To achieve an axial profile, the measurement electrodes were connected to a relay board (SainSmart) controlled by a microcontroller (Arduino), to allow switching between six electrode pairs for measurements. The cell was connected to the conductivity meter described in section 3.4, which has four inputs, two for each pair of current injecting and measurement electrodes. The complete set up is visualized in figure 15.

The sensor is used to take six experimental measurements, between measurement electrodes 1 and 2, 2 and 3 and so on. A summary of the experimental measurements with corresponding z-dimension and electrode pairs is shown in table 4.

A cone was constructed from PLA to emulate the air cone simulated in figure 14. The PLA cone was placed in the axial profiling conductivity sensor (figure 15) and the experimental results compared to that of the actual water content produced by the cone, and the simulated measurement from figure 14,
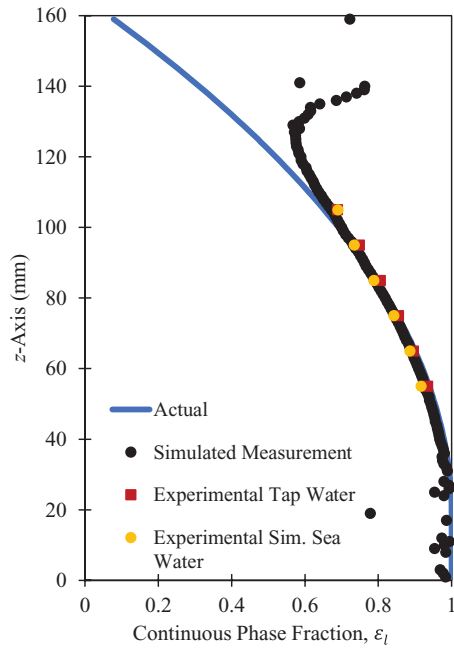
Figure 16. Experimentally measured continuous phase fraction, compared to actual and simulated continuous phase fraction measurement.

shown in figure 16 for both Montréal tap water and simulated sea water.

The change in water content as determined by the built conductivity cell was very close to that predicted by the simulation, and to the actual water content. The electronic relay was programmed to automatically switch between measurement electrode pairs to create a programmable axial profiling conductivity sensor. The results from this study show the potential for the use of this type of sensor to measure the axial change in void fraction for flowing dispersions. This is especially the case in flotation froths, where the changing water content in the froth impacts the flotation performance.

5. Conclusions

Conductivity measurements can be used to determine the continuous phase fraction in dispersions such as determining the water content in flotation froths. To do this, accurate measurements of the bulk conductivity are required. The accuracy of bulk conductivity measurements is dependent on the uniformness of the electric field generated between electrodes in the conductivity cell. To quantify the electric field uniformness, the concept of effective measure volume (EMV) was introduced with values ranging from 0 to 1, where an EMV value of 1 indicates an ideal uniform electric field. The EMV of a conductivity cell is dependent on the geometry of the electric field generating electrodes. The EMV is investigated for different conductivity cell geometries for ring electrode conductivity cell designs. The effect of EMV on bulk annular flow measurements were simulated and verified using experimental data by using PLA cylinders to emulate annular flow. It is shown that as the EMV tends towards 1, the conductivity cell tends towards no measurement error in determining bulk

continuous phase fractions. Conductivity cells that have values lower than 1 tend to produce bias in measuring the phase closer to the electrodes due to concentration of current there. This is quantified in the sum of squared residuals of the measurement, where a conductivity cell with an EMV of 0.19 has a sum of squared residual that is 638.4 times larger than a cell with an EMV of 1.00.

Conductivity cells of varying geometries were simulated, and it was determined that the electrode ring width should be minimized, and a separation-to-diameter ratio of no less than 1.0 should be used to obtain a sufficiently large EMV (of ~0.97).

Using the results from the EMV investigations, a four-probe conductivity cell is developed and tested to determine the axial-dimension profile of continuous phase fraction within the cell. The concept of EMV can be applied to the design of any bulk conductivity flow cell.

Acknowledgments

Appendix

Derivation of equation (14) to determine the continuous phase fraction from voltage drop measurements in a four-electrode conductivity cell.

Conductivity κ (mS cm^{-1}) is measured by measuring the conductance of the solution, G (mS), and the *cell constant*, A (cm), of the conductivity cell by equation (A.1):

$$\kappa = \frac{G}{A}. \tag{A.1}$$

The cell constant considers the geometry (size and spacing) of the electrodes. When the ratio of conductivities is taken, measured from the same cell, the cell constant can be ignored and the ratio of measured conductance can be used, as shown in equation (A.2):

$$\frac{\kappa_2}{\kappa_1} = \frac{\frac{G_2}{A}}{\frac{G_1}{A}} = \frac{G_2}{G_1}. \tag{A.2}$$

From equation (A.2), the relative conductivity, K can be expressed as the ratio of the bulk and continuous phase conductance:

$$K = \frac{G_{\text{bulk}}}{G_{\text{cont}}}. \tag{A.3}$$

The continuous phase fraction, $\varepsilon_{\text{l,annular}}$, is then determined by equation (A.4) [17]:

$$\varepsilon_{\text{l,annular}} = K. \tag{A.4}$$

Continuing the derivation, the measured conductance is related to the voltage drop, V (V) across the measurement electrodes, and the current flowing past the electrodes, I (mA), in eqaution (A.5).

$$G = \frac{I}{V}. \tag{A.5}$$

For the four-electrode conductivity cell simulations, the current injection is set constant, and the voltage drop across the measurement electrodes is used to determine the conductance. Substituting equation (A.5) into (A.3) for the bulk and continuous phase measurements yields equation (A.6):

$$K = \frac{G_{\text{bulk}}}{G_{\text{cont}}} = \frac{\frac{I}{V_{\text{bulk}}}}{\frac{I}{V_{\text{cont}}}} = \frac{V_{\text{cont}}}{V_{\text{bulk}}} \tag{A.6}$$

where V_{cont} (V) is the voltage drop across the electrodes measuring just the continuous phase and V_{bulk} is the voltage drop across the electrodes when measuring both phases. If equation (A.6) is substituted into equation (A.4), a relationship is formed between the continuous phase fraction and the voltage drop measurements (equation (A.7)):

$$\varepsilon_{\text{l,annular}} = \frac{V_{\text{cont}}}{V_{\text{bulk}}}. \tag{A.7}$$

ORCID iDs

L Vinnett ● https://orcid.org/0000-0001-7173-9054
O Liboiron-Ladouceur ● https://orcid.org/0000-0001-6238-5346
K E Waters ● https://orcid.org/0000-0002-8546-5688

References

[1] Lusheng Z *et al* 2012 The development of a conductance method for measuring liquid holdup in horizontal oil–water two-phase flows *Meas. Sci. Technol.* **23** 025304

[2] Lucas G P, Cory J C and Waterfall R C 2000 A six-electrode local probe for measuring solids velocity and volume fraction profiles in solids-water flows *Meas. Sci. Technol.* **11** 1498

[3] Ellis A L *et al* 2019 The hydrophobic modification of kappa carrageenan microgel particles for the stabilisation of foams *J. Colloid Interface Sci.* **538** 165–73

[4] Gomez C O and Finch J A 2007 Gas dispersion measurements in flotation cells *Int. J. Miner. Process.* **84** 51–8

[5] Vergouw J, Gomez C O and Finch J A 2004 Estimating true level in a thickener using a conductivity probe *Miner. Eng.* **17** 87–8

[6] Heiskanen K 2000 On the relationship between flotation rate and bubble surface area flux *Miner. Eng.* **13** 141–9

[7] Wills B A and Finch J A 2016 *Wills' Mineral Processing Technology* 8th edn (Boston, MA: Butterworth-Heinemann)

[8] Maxwell J C 1873 *A Treatise on Electricity and Magnetism* vol 1 (Oxford: Clarendon)

[9] Uribe-Salas A, Gomez C O and Finch J A 1994 A conductivity technique for gas and solids holdup determination in three-phase reactors *Chem. Eng. Sci.* **49** 1–10

[10] Banisi S, Finch J A and Laplante A R 1994 On-line gas and solids holdup estimation in solid-liquid-gas systems *Miner. Eng.* **7** 1099–113

[11] Miranda F J T 1996 Flow cells to measure electrical conductivity: use in estimating gas holdup in flotation systems *PhD Thesis* Department of Mining and Metallurgical Engineering, McGill University, Montreal, Canada

[12] Cortes-Lopez F 1999 Design of a gas holdup sensor for flotation diagnosis *MEng Thesis* Department of Mining and Metallurgical Engineering, McGill University, Montreal, Canada

[13] Laskowski J and Woodburn E T 1998 *Frothing in Flotation II: Recent Advances in Coal Processing* (London: Taylor and Francis)

[14] Marchese M M, Uribe-Salas A and Finch J A 1992 Measurement of gas holdup in a three-phase concurrent downflow column *Chem. Eng. Sci.* **47** 3475–82

[15] Feitosa K *et al* 2005 Electrical conductivity of dispersions: from dry foams to dilute suspensions *J. Phys.: Condens. Matter* **17** 6301

[16] Trahar W J 1981 A rational interpretation of the role of particle size in flotation *Int. J. Miner. Process.* **8** 289–327

[17] Andreussi P, Di Donfrancesco A and Messia M 1988 An impedance method for the measurement of liquid hold-up in two-phase flow *Int. J. Multiph. Flow* **14** 777–85

[18] Devia F and Fossa M 2033 Design and optimisation of impedance probes for void fraction measurements *Flow Meas. Instrum.* **14** 139–49

[19] Bruggeman D A G 1935 Berechnung verschiedener physikalischer Konstanten von heterogenen Substanzen. I. Dielektrizitätskonstanten und Leitfähigkeiten der Mischkörper aus isotropen Substanzen *Phys Ann.* **416** 636–64

[20] Jin N D *et al* 2008 Design and geometry optimization of a conductivity probe with a vertical multiple electrode array for measuring volume fraction and axial velocity of two-phase flow *Meas. Sci. Technol.* **19** 045403

[21] MathWorks 2018 *Partial Derivative Equation Toolbox* www.mathworks.com/

[22] Dichtl C, Sippel P and Krohns S 2017 Dielectric properties of 3D printed polylactic acid *Adv. Mater. Sci. Eng.* **2017** 10

[23] Pawar S D, Murugavel P and Lal D M 2009 Effect of relative humidity and sea level pressure on electrical conductivity of air over Indian Ocean *J. Geophys. Res.* **114** D02205

[24] Garcia-Vazquez V 2017 Biased four-point probe resistance *Rev. Sci. Instrum.* **88** 114701